Resonant above-threshold ionization of atomic hydrogen

Y. Gontier and M. Trahin
Service des Photons, Atomes et Molécules, Centre d'Etudes de Saclay, 91191 Gif-sur-Yvette CEDEX, France
(Received 21 October 1991)

An all-order multiphoton resonant theory for above-threshold ionization is presented within the resolvent formalism. An analytical expression displaying all the contributions to the electron yield is discussed. The theory is applied to the calculation of photoelectron energy spectra for ionization of H by picosecond and subpicosecond pulses of linearly polarized light at 608 nm, with laser intensities in the range $10^{13}-10^{14}$ W/cm^2. The role of intensity, interaction time, and transition couplings, in the resonantly enhanced electron yield coming from each (nl) intermediate state, is discussed. The modifications which affect the shape of the spectrum as the laser peak intensity increases are described in great detail. An inversion of the relative amplitudes of the resonant structures is observed. This effect is attributed to the relative dimensions of the effective interaction volumes in which the field reaches sufficient intensities to give rise to the resonances. Our results reproduce the main features of recently measured spectra [H. Rottke *et al.*, Phys. Rev. Lett. **64**, 404 (1990)].

PACS number(s): 32.80.Rm, 32.60.+i

I. INTRODUCTION

One of the most interesting effects investigated in multiphoton ionization of atoms by intense laser light is above-threshold ionization (ATI). This name refers to the absorption by an atom of more photons than the minimum number N required to reach the ionization limit. This effect has been extensively discussed in the past decade for intensities of about 10^{13} W/cm^2 and pulse widths not shorter than a few picoseconds [1]. The relevant photoelectron energy spectrum consists in equally spaced peaks whose amplitudes as well as positions depend on intensity. For intense picosecond and subpicosecond pulses recent experiments have shown that low-energy ATI peaks break up into a series of narrow lines. The origin of these new structures was ascribed to resonances induced by the field [2]. Some years ago resonant ionization in Cs was in contrast investigated by frequency tuning [3]. The process was conveniently described within the dressed-atom scheme. This model which was very fruitful to investigate resonantly enhanced multiphoton ionization (REMPI) [4] can again be invoked for resonant and nonresonant ATI processes. We recall that the dressed energies of any atomic state are obtained by adding (subtracting) the energy of $1,2,\ldots,p$ photons (multiplicities $\pm1,\pm2,\ldots,\pm p$) to the usual intensity-dependent energy of that state. The plots of the dressed energies of the atoms as functions of the intensity provide a network of curves representing the dynamical atomic spectrum. Thus the resonances can be interpreted in terms of crossings (anticrossings) of any two energy curves. Such a representation holds for levels belonging to the discrete and the continuum spectrum. The only difference is that, in the latter case, the levels are infinitely degenerated. Within this framework the various processes can be classified into (i) those which are due to the crossing (anticrossing) of two discrete levels (ii) those coming from the crossing of discrete and continuum levels (ATI without resonant structures), and (iii) those resulting from the combination of the two preceding ones. The last case characterizes what we have called resonantly enhanced above-threshold ionization (REATI). In contrast to REMPI which was obtained by frequency tuning, REATI appears at fixed photon energy, when the ac Stark shift of any discrete level compensates the energy gap between that level and one of the initial dressed states. The consequence is that many resonances can successively be tuned, at some intensities I_R during the rising and the falling of the pulse. This explains why the ATI spectrum acquires resonant structures whose positions are characterized by intensities I_R but which are not sensitive to the pulse amplitude I_M. The counterpart of this effect is that the beam focusing now plays an important role. Since these intensities I_R cannot be reached at every point of the focal region, we must determine the domain where the laser intensity is at least equal to each resonant one. In other words, one must determine an effective interaction volume V_R for each resonance. The interaction space is split into a set of nested volumes characterized by decreasing values of the intensity I_R. The V_R's and consequently the resonant enhanced yield grow with I_M. In Sec. II the theoretical model for multiresonant ionization of atoms is discussed by making intensive use of the resolvent operator $G(z)$. By resorting to nonperturbative expressions of the shift operator $R(z)$ previously obtained in the general case, we formulate the problem of REATI within the framework of a nonperturbative theory. A method for straightforwardly writing down the matrix elements of $G(z)$ is proposed. This treatment provides a good opportunity to display all the resonant and multiresonant channels which contribute to the ionization process. In the case of laser pulse of moderate intensity ($\leq 10^{14}$ W/cm^2), a simplified expression for the probability density is derived from the general theory. In Sec. III our results are used to study REATI for hydrogen. The intensity dependence of the energy spectrum of the photoelectrons is investigated in the case of 0.5-psec pulses of linearly polarized light at

608 nm for intensities up to 10^{14} W/cm^2. Our results are in agreement with experimental data in H. The effects coming from the expansion of the interaction volume on the production of the expected resonant electrons, and also of the nonresonant electrons (ATI), are carefully examined. At low intensity we show that the amplitude of the peaks which arise from resonances with the F levels increases with the electron energy E. At higher intensity we observe, in agreement with experiments, an inversion in the behavior of the peak heights which now decrease with energy E. Finally, we report the effect of the pulse width on electron spectra computed at fixed laser energy. For pulse durations over the range 0.3–2 psec, the results display a rapid modification in the shape of the curves which evolves from the standard ATI towards the typical resonant spectrum.

II. BASIC MULTIRESONANT IONIZATION PROBABILITY

Advances in laser technology have made possible the generation of ultraintense fields via subpicosecond pulses. The structures of atoms embedded in such radiation fields undergo strong distortions. Under these circumstances, the lowest-order perturbation theory (LOPT) cannot lead to correct transition amplitudes. Nonperturbative approaches for solving the Schrödinger equation of the atom in an intense field have recently been proposed [5]. Some years ago we have shown how the standard perturbation series could be exactly summed in order to express the ionization probability in the form of rapidly converging continued fractions [6]. Theoretically, these fractions may be computed up to any degree of accuracy. In the present work, the expressions required for computations are written down in bringing out the role played by the most prominent terms. By the time the laser is switched on, atomic levels of well-defined multiplicities can be shifted into resonance. Within the previous energy representation, this situation can be viewed as being a crossing (anticrossing) of levels belonging to different multiplicities. For example, in a given ionization channel, the ground state $|a\rangle_m$, the discrete state $|b\rangle_n$, and the continuum $|c\rangle_q$ of multiplicities m, n, and q, respectively, can be energetically degenerated. The energy difference $E_{ab}=E_a-E_b$ occurring in the expressions of the matrix elements is so small that no satisfactory convergence can be reached in numerical calculations. This difficulty is overcome by defining the subspace ($\mathcal{E}$) which is spanned by all the degenerate resonant states. Then a new expression of the ionization probability is set up in the basis of all the remaining eigenfunctions. In doing so, REATI processes require the calculation of continued fractions whose convergence is rapidly obtained after few iterations.

A. Theoretical framework

Within the resolvent formalism, the probability amplitude for producing an electron in the continuum (c) at time t reads

$$U_{ca}(t)=\frac{1}{2\pi i}\oint G_{ca}(z)e^{-izt}dz \ . \tag{2.1}$$

The computation of this quantity requires the evaluation of a contour integral in the complex plane. This can be done within the subspace ($\mathcal{E}$) by calculating the residues corresponding to the principal poles, i.e., the poles which provide the major contribution to $G(z)$. For transitions from the ground state $|a\rangle$ to any final state $|c\rangle$ we shall assume that M states can provide resonances (for brevity, the multiplicities will not be explicitly written but can be restored if necessary). The projectors P and Q onto and outside the $(M+2)$-dimensional subspace ($\mathcal{E}$) are defined as

$$P=|a\rangle\langle a|+\sum_{j=1}^{M}|b_j\rangle\langle b_j|+|c\rangle\langle c| \ , \tag{2.2a}$$

and

$$Q=1-P \ , \tag{2.2b}$$

with the obvious relations $P^2=P$ and $Q^2=Q$, the restriction $\bar{G}(z)$ of $G(z)=1/(z-H)$ to the subspace ($\mathcal{E}$) is

$$\bar{G}(z)=\frac{1}{z-H_0-\bar{R}(z)} \ , \tag{2.3}$$

where

$$\bar{G}(z)=PG(z)P \ , \tag{2.4a}$$

$$\bar{R}(z)=PR(z)P \ , \tag{2.4b}$$

and H_0 is the unperturbed Hamiltonian of the system atom plus field. In Eq. (2.4b) $R(z)$ can be expressed in the form of a power series of the interaction V as

$$R(z)=V+V\frac{Q}{z-H_0}V+V\frac{Q}{z-H_0}V\frac{Q}{z-H_0}V+\cdots \ . \tag{2.5}$$

To work within a nonperturbative scheme, the series of Eq. (2.5) must be summed. This summation has been done in previous accounts [6]. We only recall the general operator expressions thus obtained. One distinguishes the diagonal and the nondiagonal expressions of $R(z)$ accounting for no net photon absorption and for the absorption of $N+S$ photons, respectively. The number of photons required for ionization is N, while S photons are absorbed in the continuum. One has

$$R_{\text{diag}}(z)=(V^-\bar{\tau}_\square\bar{B}\bar{\tau}_\phi+V^+\bar{\tau}_\square\bar{A}\bar{\tau}_0)(z-H_0) \ , \tag{2.6a}$$

$$R^{(N+S)}_{\text{nondiag}}(z)=[V^+\bar{\tau}_\square(\bar{A}\bar{\tau}_0)^{N+S+1}+V^-\bar{\tau}_\square(\bar{A}\bar{\tau}_0)^{(N+S-1)}](z-H_0) \ . \tag{2.6b}$$

In Eqs. (2.6) $\bar{\tau}_0$, $\bar{\tau}_\phi$, and $\bar{\tau}_\square$ are the following continued fractions of $\bar{A}=QV^-$ and $\bar{B}=QV^+$:

$$\bar{\tau}_0=\frac{1}{z-H_0-\bar{A}\bar{\tau}_0\bar{B}} \ , \tag{2.7a}$$

$$\bar{\tau}_\phi=\frac{1}{z-H_0-\bar{B}\bar{\tau}_\phi\bar{A}} \ , \tag{2.7b}$$

$$\bar{\tau}_{\square}=\frac{1}{z-H_0-\bar{A}\bar{\tau}_0\bar{B}-\bar{B}\bar{\tau}_{\varnothing}\bar{A}}\ , \tag{2.7c}$$

and V^- and V^+ are the absorption and the emission operators of a photon, respectively ($V=V^++V^-$). According to Eqs. (2.3) and (2.7), one has to invert the matrix $[z-H_0-\bar{R}(z)]$ whose size is large when ($\mathcal{E}$) is a many-dimensional space. As a consequence, the expression of any matrix element of $\bar{G}(z)$ is prohibitively complicated.

B. Cascade equations

The above-mentioned difficulty can be tackled by resorting to the following method which enables one to write any matrix elements of $\bar{G}(z)$ in a systematic and compact form. We define a set of M operators $W^{(1)}(z), W^{(2)}(z), \ldots, W^{(M)}(z)$ acting on the $(M+2)$-dimensional subspace ($\mathcal{E}$) and related to each other by the following system of M cascade equations:

$$W^{(M)}(z)=W^{(M-1)}(z)+W^{(M-1)}(z)\frac{|b_M\rangle\langle b_M|}{z-E_{b_M}-W^{(M-1)}_{b_Mb_M}(z)}\times W^{(M-1)}(z)\ , \tag{2.8a}$$

$$W^{(M-1)}(z)=W^{(M-2)}(z)+W^{(M-2)}(z)\frac{|b_{M-1}\rangle\langle b_{M-1}|}{z-E_{b_{M-1}}-W^{(M-2)}_{b_{M-1}b_{M-1}}(z)}\times W^{(M-2)}(z)\ , \tag{2.8b}$$

$$W^{(k)}(z)=W^{(k-1)}(z)+W^{(k-1)}(z)\frac{|b_k\rangle\langle k_k|}{z-E_{b_k}-W^{(k-1)}_{b_kb_k}(z)}\times W^{(k-1)}(z)\ , \tag{2.8c}$$

$$W^{(1)}(z)=R(z)+R(z)\frac{|b_1\rangle\langle b_1|}{z-E_{b_1}-R_{b_1b_1}(z)}R(z)\ . \tag{2.8d}$$

For convenience the subscripts labeling the resonant states and the superscripts denoting the operators $W(z)$ have been written according to decreasing orders. In fact all these operators ($|b_k\rangle$ and $W^{(k)}(z)$; $k=1,2,\ldots,M$) can be considered in any order. The only requirement is that each of them must occur once. It may be shown that the matrix elements of $\bar{G}(z)$ can be simply expressed in terms of $W^{(M)}(z)$. The diagonal matrix element with respect to any state $|j\rangle$ of ($\mathcal{E}$) is given by

$$G_{jj}(z)=\frac{1}{z-E_j-W^{(M)}_{jj}(z)}\ , \tag{2.9}$$

while the nondiagonal matrix element taken over any two states $|i\rangle$ and $|j\rangle$ is

$$G_{ij}(z)=\frac{W^{(M)}_{ij}(z)}{[z-E_i-W^{(M)}_{ii}(z)][z-E_j-W^{(M)}_{jj}(z)]-W^{(M)}_{ij}(z)W^{(M)}_{ji}(z)}\ . \tag{2.10}$$

The result of Eq. (2.10) will not be demonstrated here but it can be checked by straightforward algebra. The expression of Eq. (2.10) is a generalization to $(M+2)$ levels of the formula encountered in two-level problems. Thus any nondiagonal matrix element of $\bar{G}(z)$ can be obtained by substituting $W^{(M)}(z)$ for $R(z)$ in a two-level-like formula. For any transition ($|i\rangle\rightarrow|j\rangle$) it must be noted that the operator $W^{(M)}(z)$ is expressed as a function of couplings between all states belonging to ($\mathcal{E}$) except $|i\rangle$ and $|j\rangle$. In the following, we should refer to the subspace $\mathcal{E}_{ij}$ which is spanned by these M coupled states.

The evaluation of the contour integral on the right-hand side of Eq. (2.1) requires the computation of the contributions coming from the $(M+2)$ poles implicitly enclosed in the expression of $\bar{G}_{ij}(z)$. In practice, the values of these $(M+2)$ poles are obtained by determining the roots of the algebraic equation

$$K^{(M-1)}_M(z)[X^{(M)}_i(z)X^{(M)}_j(z)-W^{(M)}_{ij}(z)W^{(M)}_{ji}(z)]=0\ . \tag{2.11}$$

Equation (2.11) is obtained by multiplying both numerator and denominator of Eq. (2.10) by the product of energy functions

$$K^{(M-1)}_M(z)=[X^{(0)}_1(z)X^{(1)}_2(z)\cdots X^{(M-1)}_M(z)]\ ,$$

where $X^{(0)}_q(z)=z-E_q-R_{qq}(z)$ and $X^{(k)}_q(z)=z-E_q-W^{(k)}_{qq}(z)$. In doing so, all the poles coming from Eq. (2.11) are treated on an equal footing. By considering Eq. (2.11) instead of the energy denominator of Eq. (2.10) we rebuild the determinant arising from the computation of $[z-H_0-\bar{R}(z)]^{-1}$. Since all possible resonances have been extracted from $R_{pq}(z)$, Eq. (2.11) is a polynomial of degree $(M+2)$ in z, whose coefficients are slowly varying functions of z. The numerical computation of the poles is greatly simplified by making use of this remark. The numerator of Eq. (2.10) combines with $K^{(M-1)}_M(z)$ to give the matrix element

$$\mathcal{N}_{ij}(z)=K^{(M-1)}_M(z)W^{(M)}_{ij}(z)\ , \tag{2.12}$$

from which all the channels contributing to the transition $|i\rangle\rightarrow|j\rangle$ can be defined. By expressing $\mathcal{N}_{ij}(z)$ in terms of $R(z)$, Eq. (2.12) may be arranged in the following compact form:

$$\mathcal{N}_{ij}(z)=R_{ij}(z)\left[\prod_{q=1}^{M}X_q^{(0)}(z)-O^{(M)}(z)\right]+\sum_{k=1}^{M}R_{ik}(z)R_{kj}(z)\left[\prod_{\substack{q=1\\(q\neq k)}}^{M-1}X_q^{(0)}(z)-O_k^{(M-1)}(z)\right]$$
$$+\sum_{\text{perm}\{k,p\}}[R_{ik}(z)R_{kp}(z)R_{pj}(z)]\left[\prod_{\substack{q=1\\(q\neq k,p)}}^{M-2}X_q^{(0)}(z)-O_{kp}^{(M-2)}(z)\right]$$
$$+\cdots+\sum_{\text{perm}\{1,2,3,\ldots,M\}}[R_{i1}(z)R_{12}(z)\cdots R_{M-1,M}(z)R_{Mj}(z)]\,, \tag{2.13}$$

where the symbol $\sum_{\text{perm}\{k,p,\ldots,s\}}$ indicates that one must sum over all the permutations of any set of states $\{k,p,\ldots,s\}$ belonging to $\mathcal{E}_{ij}$. The functions $O^{(s)}(z)$ are finite sums of the diagonal element of $R(z)$-operator products coupling the resonant states of $(\mathcal{E}_{ij})$. For example, one has

$$O^{(M)}(z)=\sum_{\text{perm}\{m,n\}}[R_{mn}(z)R_{nm}(z)]\prod_{\substack{k=1\\(k\neq m,n)}}^{M-2}X_k^{(0)}+\sum_{\text{perm}\{m,n,p,\}}[R_{mn}(z)R_{np}(z)R_{pm}(z)]\prod_{\substack{k=1\\k\neq n,m,p}}^{M-3}X_k^{(0)}+\cdots$$
$$+\sum_{\text{perm}\{n,m,p,\ldots,s\}}[R_{mn}(z)R_{np}(z)\cdots R_{qs}(z)R_{sm}(z)]\,, \tag{2.14}$$

and also $O^{(1)}\equiv 0$. From Eq. (2.14) we can deduce that $O^{(M)}(z)$ is a higher-order correction to the nonresonant transition term $R_{ij}(z)$. In the same way $O_k^{(M-1)}(z)$ will be a correction for the matrix element $R_{ik}(z)R_{kj}(z)$ and so on. Although some terms in $O^{(s)}(z)$ are resonant, the order of the relevant matrix elements is so high that $O^{(s)}(z)$ can be neglected for light fields at moderate intensity ($<10^{15}$ W/cm^2). For more intense radiations these terms may be calculated without further difficulties.

C. Discussion

Now that we have obtained a useful expression for the matrix elements $\mathcal{N}_{ij}(z)$ we would like to discuss the meaning of the terms contained herein. The right-hand side of Eq. (2.13) explicitly exhibits all the contributions coming from the $(M+2)$ resonant states of $(\mathcal{E})$.

(i) The first term $R_{ij}(z)$ gives the contributions to $G_{ij}(z)$ coming from all the nonresonant channels coupling the states $|i\rangle$ and $|j\rangle$ (ATI process).

(ii) The second term $R_{ik}(z)R_{kj}(z)$ represents the channels which only include one resonant state of $(\mathcal{E}_{ij})$. Note that each resonant level $|k\rangle$ crosses $|i\rangle$ and $|j\rangle$, at time t_k, for a laser intensity $I_R(t_k)$.

(iii) The third term $R_{ik}(z)R_{kp}(z)R_{pj}(z)$ appears when the transition $|i\rangle\rightarrow|j\rangle$ takes place via two resonant states. Usually the resonances occur at two different times t_k and t_p with the relevant intensities $I_R(t_k)$ and $I_R(t_p)$, respectively. These terms will be of the same order of magnitude as those considered in (ii), if the parities of $|k\rangle$ and $|p\rangle$ do not differ by more than one unit. Otherwise, their contributions will be of higher order, as deduced from the expression of $R(z)$ in Eq. (2.6). It may happen that time t_k is approximately equal to t_p. Then we will have to deal with a double-resonant term which can bring about an important increase of the contribution to $G_{ij}(z)$.

(iv) The last term in eq. (2.13) represents all the channels coupling the states $|i\rangle$ and $|j\rangle$ via all the resonant states of $(\mathcal{E}_{ij})$. The remarks in (iii) apply to this case.

In addition we shall note that for a given M, the number of terms in Eq. (2.13) remains finite, while it grows with M.

Once the poles are known by solving Eq. (2.11), $G_{ij}(z)$ is obtained from

$$G_{ij}(z)=\frac{\mathcal{N}_{ij}(z)}{(z-z_i)X_1^0(z)X_2^0(z)\cdots X_M^0(z)(z-z_j)} \tag{2.15}$$

and the calculation can be achieved up to any degree of accuracy. We note that $R(z)$ is a rapidly convergent continued fraction which is computed in a finite basis of eigenfunctions of the Hamiltonian H_0 excluding those of the subspace $(\mathcal{E})$. The precision reached in the evaluation of $R(z)$ may be easily controlled by varying the number of states in the basis, and by carrying out more iterations in the computation of the continued fraction. In many realistic cases, the evaluation of $\mathcal{N}_{ij}(z)$ reduces to the calculation of some prominent terms in Eq. (2.13), which are selected by simple physical consideration.

The previous treatment can be readily applied to the interaction of two discrete states $|a\rangle$ and $|b\rangle$, with a state $|c(\alpha,E)\rangle$, belonging to the set of energy states $|c(\alpha,E_1)\rangle,\ldots,|c(\alpha,E_n)\rangle$, generated by the discretization of the continuum characterized by the quantum number α. If a careful investigation of the perturbed energy spectrum reveals that the state $|b\rangle$ may be shifted into resonance at intensity $I_R(t_b)$, the main contribution to the transition amplitude $U_{ca}(\alpha,E,t_b)$ will be obviously given by the resonant term $R_{cb}(z)R_{ba}(z)$ of Eq. (2.13). The corrections coming from the nonresonant channels $R_{ca}(z)$ are very small and it may be expected that those arising from the terms $\sum_S R_{cb}R_{bS}R_{Sa}$ could be neglected. Indeed the contributions of these last channels are of

higher order since they involve more absorptions than the minimum number required for the resonant transition ($a \rightarrow c$). Moreover, we note that the level (b) does not cross the level (s) at intensity $I_R(t_b)$. It is clear that this off-resonance situation minimizes the contributions coming from $R_{cb}R_{bS}R_{Sa}$. For the case under consideration, the present discussion leads to the following expression for the transition amplitude:

$$U_{ca}(\alpha,E_c,t)=\frac{R_{cb}(z_a)R_{ba}(z_a)}{(\tilde{E}_{ab}-i\Gamma_{ab})(\tilde{E}_{ac}-i\Gamma_{ac})}e^{-i\tilde{E}_a t-\Gamma_a t}+\frac{R_{cb}(z_b)R_{ba}(z_b)}{(\tilde{E}_{ba}-i\Gamma_{ba})(\tilde{E}_{bc}-i\Gamma_{bc})}e^{-i\tilde{E}_b t-\Gamma_b t}$$
$$+\frac{R_{cb}(z_c)R_{ba}(z_c)}{(\tilde{E}_{ca}-i\Gamma_{ca})(\tilde{E}_{cb}-i\Gamma_{cb})}e^{-i\tilde{E}_c t-\Gamma_c t}. \tag{2.16}$$

In Eq. (2.16) the complex energy $z_j=E_j+\Delta_j-i\Gamma_j$ of the jth pole is expressed in terms of the dynamic Stark shift $(\Delta_j-i\Gamma_j)$. We have used the notations

$$z_j=\tilde{E}_j-i\Gamma_j$$

for the energy of the main poles and

$$z_i-z_j=\tilde{E}_{ij}-i\Gamma_{ij}$$

for energy differences.

The multiresonant character of the interaction may assume several aspects: (i) Resonances can appear in several distinct channels $|a\rangle \rightarrow |c(\alpha_p,E)\rangle$, and (ii) in a given channel $|a\rangle \rightarrow |c(\alpha,E)\rangle$ several states can be successively shifted into resonance at appropriate times.

In both cases, ionization may be described with the help of expressions like that of Eq. (2.16). The transition amplitude $U_{ca}(\alpha,E,t)$ is expressed in terms of the two fractions $F_{ab}=(\tilde{E}_{ab}-i\Gamma_{ab})^{-1}$ and $F_{ac}=(\tilde{E}_{ac}-i\Gamma_{ac})^{-1}$. The former leads to the conventional resonance curve coming from the level crossing of two discrete states $|a\rangle$ and $|b\rangle$. At the position of the maximum, the intensity $I_R(t_b)$ is determined by the relation $\tilde{E}_{ab}=0$. The amplitude of F_{ab} is a rapidly varying function of the intensity around $I_R(t_b)$. This variation is somewhat moderated by the presence of F_{ac}. In fact, inspection of Eq. (2.16) indicates that the dressed energy level $[E_a+\Delta_a+(N+1)\omega]$, involved by an $(N+1)$-photon ionization process (N-photon resonant), lies in the continuum spectrum inside an energy range Ω having the width $2\Gamma_{ac}$. For each energy value taken within Ω, it corresponds to a value of the function F_{ac} which acts as a weighting factor for the transition amplitude. This explains why the behavior of the probability is not only governed by the resonant factor F_{ab},but also depends on the weighting function F_{ac}. In Eq. (2.16) the function F_{ac} is typical of the probability of emitting an electron at intensity $I_R(t)$ within the energy range Ω.

III. IONIZATION OF ATOMIC HYDROGEN AT 608 nm

The method we have described in Sec. II has been readily applied to discussion of above-threshold ionization of atomic hydrogen. We have computed the energy spectrum of photoelectrons produced by sharp Gaussian pulses of linearly polarized light at 608 nm. The pulse duration is around $d=0.5$ psec and the laser peak intensity I_M within the range ($\sim 10^{13}$–10^{14} W/cm^2). For these 250 optical cycle pulses, the laser bandwidth is about 4 meV. This value is very small compared to both laser frequency and energy gaps separating any resonant state from the next one. For this reason, the electron spectrum does not seem to be affected by the laser bandwidth which will be neglected in the calculations.

The experimental results obtained in xenon [2,7,8] and hydrogen [9] indicate that these spectra may be reasonably interpreted by assuming that the whole manifold of states, as well as the continuum limit, would be shifted with the same intensity dependence. This tendency is confirmed by the angular distributions of photoelectrons which reveal that for intensities as high as 10^{14} W/cm^2, the ionization potential of the atom increases by an amount approximately equal to the quiver energy [10]. This remark suggests that the electron spectrum may be simply computed by using the second-order perturbative values of the complex shift given in Table I [11]. In doing so, we assume that the continued fractions which express $R_{\text{diag}}(z)$ [Eq. (2.6(a)], can be truncated after one division only. Within this approximation we neglect the contributions of many couplings with far-off dressed energy states and we restrict the ways the photons are absorbed and emitted; but the remaining terms in the perturbative expansion of $U_{ca}(E,t)$ are indeed infinite in number. We should see that, except for the $4P$ state, the values of the shifts and broadenings reported in Table I have allowed us to assign well-defined states to the new structures observed in the electron spectra. Note that by performing Floquet calculations of the quasienergies of various sublevels of atomic hydrogen, Dörr, Potvliege, and Shakeshaft [12] have investigated the modification of the spectrum due to the laser field. From the results published at 616 nm, it appears that, among the resonant states we consider, only the $4P$ and the $4F$ states have shifts which appreciably deviate from the linear intensity behavior we use. The comparison done in Fig. 2 between the experimental data and the theoretical electron spectrum computed by using the second-order term of the perturbative expansion of the shift [Eq. (2.5)] gives a satisfactory account of the approximation used. Our results are not surprising since the $I_R(t)$ values for the F series spread within the moderate intensity range $[(3-5)\times 10^{13}$ W/cm$^2]$.

TABLE I. Intensity values I_R (W/cm^2) required to produce electrons at the energies E_R (eV) by N-photon-ionization processes involving resonances on the nl energy level. α_{nl} and β_{nl} are the values of the level shifts and the level widths divided by intensity, respectively. The numbers in brackets are powers of 10.

nl	N	I_R	E_R	α_{nl}	β_{nl}
$6P$	8	2.842	1.71	1.33 [−15]	6.85 [−17]
$6F$	8	3.042	1.64	1.24 [−15]	1.08 [−17]
$5P$	8	3.107	1.62	1.41 [−15]	1.19 [−16]
$4P$	8	3.176	1.59	1.73 [−15]	2.37 [−16]
$5F$	8	3.556	1.46	1.23 [−15]	1.73 [−17]
$4F$	8	4.515	1.12	1.21 [−15]	2.75 [−17]
$6G$	9	8.79	1.65	1.26 [−15]	1.79 [−18]
$5G$	9	9.29	1.47	1.26 [−15]	2.02 [−18]

A. Graphic representation

A useful representation of the mechanism producing the photoelectron spectra is depicted in Fig. 1. The real part of the energy of the dressed ground states $(\tilde{E}_0+p\omega)$ has been drawn as a function of intensity. The discretized continuum states $|\alpha,E\rangle$ of energy E are plotted parallel to the continuum limit defined by $I/I_0\omega^2$ ($I_0=14.038\times10^{16}$ W/cm^2). As the laser intensity increases on the rising edge of the pulse, the atom ionizes by absorption of seven photons at intensities $I_1<I_7^L$ ($I_7^L=1.91\times10^{13}$ W/cm^2), eight photons at intensities in the range $I_7^L<I_2<I_8^L$ ($I_8^L=7.68\times10^{13}$ W/cm^2), and nine photons when $I_8^L<I_3<I_9^L$ ($I_9^L=1.34\times10^{14}$ W/cm^2). In Fig. 1(a) one observes that electrons of energy E_1 can be produced at intensity I_1 by seven-order processes or at intensity I_2 by eight-order processes, etc. These electrons are found in the first ATI peak. Electrons of energies $E_2=E_1+\omega, E_3=E_1+2\omega, \ldots$ are also created. The former, which lie in the second peak, are generated at intensity I_1 by eight-order processes and at intensity I_2 by nine-order processes, etc. In the same way electrons of energy E_3 feed the third ATI peak. The situation has been described in a previous paper [13] where it has been shown that the experimental results were in good agreement with the theoretical predictions.

In the case under consideration some discrete states $|k\rangle$ are successively shifted into resonance when the intensity reaches characteristics values $I_R^{(k)}(t)$ which cancel the energy detuning.

$$E_0-E_k+(p-1)\omega+(\alpha_0-\alpha_k)I_R^{(k)}=0\ , \tag{3.1}$$

where the α_j's denote the rates Δ_j/I and E_0 represents the ground-state energy. Since the $(P\rightarrow D)$ couplings are smaller than those corresponding to $(F\rightarrow G)$ and $(G\rightarrow H)$ transitions [14], we shall restrict the discussion to the effects produced by the resonances involving the states of the F and G series. When the light pulse sweeps the intensity $I_R^{(k)}$ of Table I, the $6F$, $5F$, and $4F$ levels (odd parity) are successively shifted into resonance with the dressed ground state of energy $(\tilde{E}_0+7\omega)$. At higher intensities, the $6G$ and $5G$ levels will in turn come into resonance with the state of energy $(\tilde{E}_0+8\omega)$. The curve crossings of these dressed atomic levels can be seen in Fig. 1(b). The atom ionizes for one more photon absorption and the free electron acquires the kinetic energy

$$E_k^R=E_0+p\omega+(\alpha_0-1/I_0\omega^2)I_R^{(k)}\ , \tag{3.2}$$

in the continuum spectrum ($p=8,9$). As for the ATI peaks in Fig. 1(a), we should note that a part of the electron populations at energies E_4, E_5, and E_6 may be generated from higher-order processes. Since the electron energy is tied to the resonant intensity $I_R^{(k)}$ according to Eq. (3.2), the position of the peak is independent of the pulse characteristics. Our results in Table I show that the $4F$ peak, at 1.12 eV, is well separated from the $5F$ peak at 1.46 eV, and from the $6F$ peak, at 1.64 eV. The last two peaks are blended with the $5G$ and the $6G$ peaks, respectively. At higher intensities we shall note that the α_js will become intensity dependent. The real part of the energies E_j will no longer be represented by straight lines but by distorted curves. However, in the modified graphic representation, the discussion can be done in a way very similar to the above-mentioned one. Now it becomes interesting to compare the relative amplitudes of the peaks emerging in the spectrum. The probability density of finding an electron in the αth continuum, at time t, with an energy lying within $(E-dE)$ and $(E+dE)$ can be written as

$$D_\alpha^{(k)}(E,t)=|U_{\alpha E,0}^{(k)}(E,t)|^2\ , \tag{3.3}$$

where the evolution operator $U_{\alpha E,0}^{(k)}(E,t)$ is given by Eq. (2.14). Since the width of the ground state Γ_0 is smaller than Γ_b and Γ_c, the largest contribution to $U_{\alpha E,0}^{(k)}(E,t)$ comes from the first term in the right-hand side of Eq. (2.14). Thus the probability density reduces to

$$D_\alpha^{(k)}(E,t)\sim\frac{R_{\alpha E,k}^2(\tilde{E}_0)R_{k0}^2(\tilde{E}_0)}{(\tilde{E}_{0k}^2+\Gamma_k^2)(\tilde{E}_{0c}^2+\Gamma_c^2)}\exp(-2\Gamma_0 t)\ . \tag{3.4}$$

This simplified expression indicates that the peak amplitude increases with the intensity-dependent matrix elements $R^2(\tilde{E}_0)$, but exponentially diminishes for increasing values of the damping term Γ_0 as well as the time t. Thus it may be expected that the electron enhancement will be more favorable for the F peaks than for the G peaks. Note that, in the case of weak laser field, Eq. (3.4) leads to the well-known expression of the lowest-order

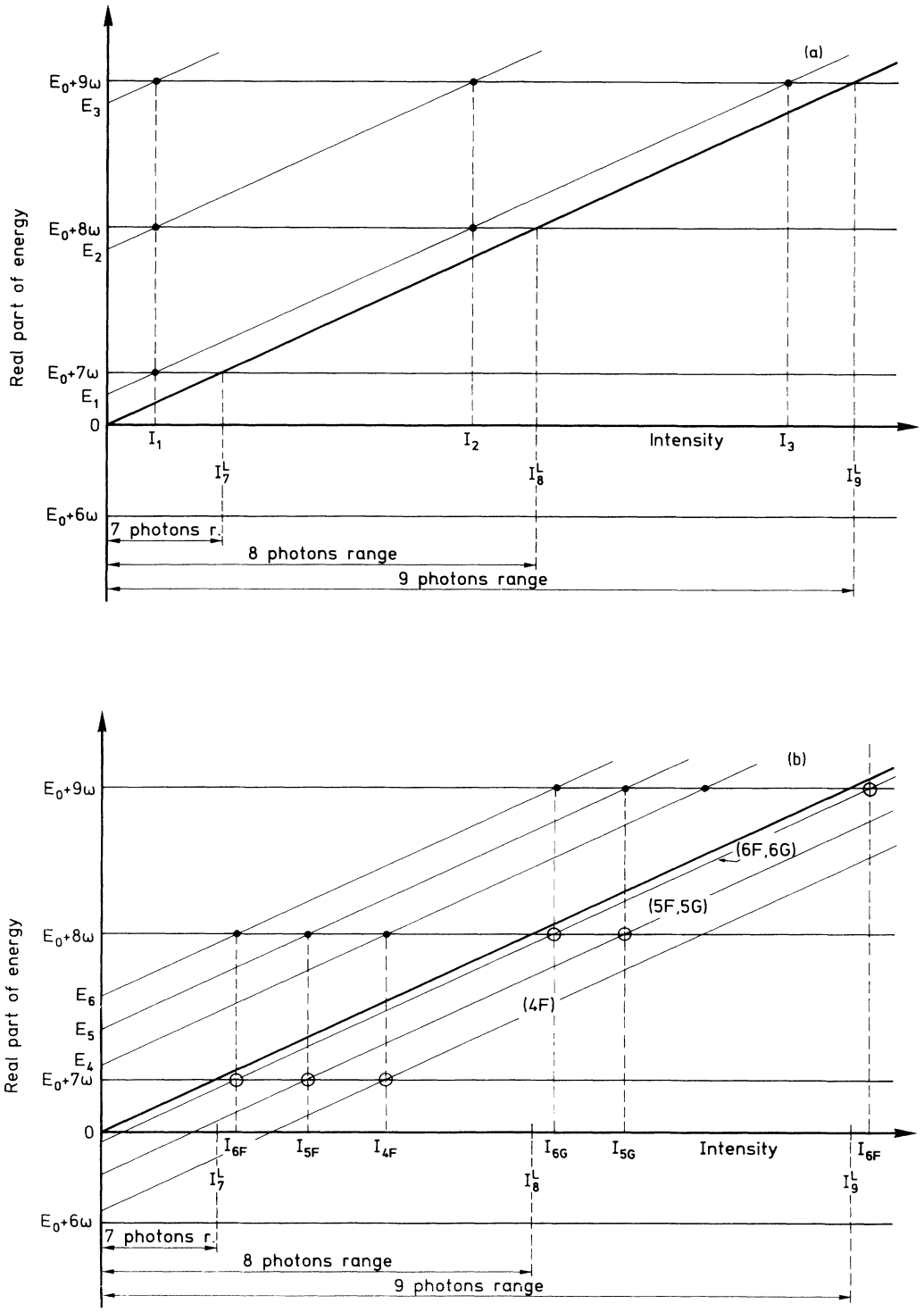

FIG. 1. (a) Diagram of the energies of a dressed atom as a function of intensity in the region where crossings give rise to ATI processes (arbitrary units). Slanted lines represent the continuum levels of energy 0, E_1, E_2, and E_3, respectively. Horizontal lines are the energies of the ground state dressed by seven, eight, and nine photons. I_1, I_2, and I_3 are the intensities at which electrons of energies E_1, $E_2=E_1+\omega$, and $E_3=E_1+2\omega$ can be produced in the first, the second, and the third ATI peaks. Solid black circles denote the level crossings where the electrons are created. I_7^L, I_8^L, and I_9^L are the threshold intensities for the seventh-, eighth-, and ninth-order process, respectively. (b) Same as 1(a). The energy levels $4F$, $5F$, $5G$, $6F$, and $6G$ have been plotted parallel to the continuum limit (arbitrary scale) (the $5F$ and $6F$ states mingle with the $5G$ and $6G$, respectively). I_{4F}, I_{5F}, and I_{5G}, I_{6F}, and I_{5G} are the intensities giving rise to resonant structures around energies E_4, E_5, and E_6, respectively. The crossings of the resonant states are represented by open circles.

ionization rate. Finally, the electron population generated, at time t, in the k-resonant peak is

$$N^{(k)}(t)=N_0(t)\int_0^\infty \sum_\alpha D_\alpha^{(k)}(E,t)dE \ , \tag{3.5}$$

where $N_0(t)$ is the number of atoms in the ground state. One aspect of calculations for ATI processes is that a theoretical estimate of the electron populations depends on the parameters of the beam focusing lens. In the following we investigate the effects of the general realistic pulse shape

$$I(R,Z,t)=I_M\frac{\exp[-R^2/(1+Z^2)]}{(1+Z^2)} \times\exp[-0.693(t-t_0)^2/\tau^2] \ , \tag{3.6}$$

where I_M is the maximum intensity at the focus, $R=0.053r$ μm, and $Z=3.6z$ mm for a focus diameter of 53 μm. R and Z are the usual dimensionless cylindrical coordinates and 2τ represents the pulse width at half maximum. Because of the spatiotemporal structure of the laser pulse, the number of electrons $n_e(E,r,z,t)$ at energy E must be calculated in each of the elementary cells within the interaction volume [15]. Since the resonance involving $|k\rangle$ occurs at a well-defined intensity $I_R^{(k)}(t)$, the electron population $\bar{n}_e(E_k)$ obtained after summation over space and time, only comes from the atoms within an effective volume V_k. This volume is determined by bringing together all the cells crossed by $I_R^{(k)}(t)$. Obviously the V_k's decrease as the relevant intensities $I_R^{(k)}$ increase. The volumes satisfy the condition $V_{6F}>V_{5F}>V_{4F}>V_{6G}>V_{5G}$ in such a way that V_{5G} is a part of V_{6G} which is a part of V_{4F} and so on.

Note that (i) at time t, the number of atoms $n_0(z,r,t)$ varies from one cell to another; (ii) the effective focal volume V_k increases with the laser peak intensity I_M; and (iii) the electron populations $\bar{n}_e(E_k)$ are accurately computed from the elementary cells. The V_k's are only used to make the discussion easier. The electrons emitted at the highest intensities would be generated near the focus or along the z axis. In contrast, the electrons producing the standard nonresonant ATI peaks would be created in the whole interaction volume surrounding all the V_k's.

B. Results and discussions

The electron spectrum obtained with a laser peak intensity of 10^{14} W/cm^2 and a 0.5-psec pulse duration is shown in Fig. 2 (solid line). The curve represents the rate $N_{el}(E)$ of the number of electrons $\bar{n}_e(E)$ created (at the end of the pulse) with an energy lying within $E-dE$ and $E+dE$, normalized with respect to the number of electrons $\bar{n}_e(E_{4F})$ at the maximum amplitude of the $4F$ peak. This normalization will be kept in the following. The calculations lead to three resonant structures with decreasing amplitudes as the electron energy increases. The $4F$ peak, at $E=1.12$ eV, is the most prominent one (the width is 0.1 eV). Theoretically, the next two peaks are produced by the mixing of electrons coming from eight- and nine-photon resonant processes. However, the computations show that only a few electrons are produced through the channels via G-resonant states which are introduced by nine-photon ionization processes. Note that the depletion due to resonant F states also reduces the possibilities of producing electrons from the $6G$ and $5G$ eight-photon resonances with occur at higher intensities. Thus from our calculations the three peaks in Fig. 2 reproduce the effect of resonances with the $4F$, $5F$, and $6F$ levels, respectively. On the low-energy side, around 0.41 eV, we observe the presence of a little hump due to a relatively small amount of nonresonant electrons generated in the first ATI peak by seven-photon-ionization process. As expected from the increase of the ionization potential, this peak is shifted towards lower energies from the theoretical unshifted position at 0.676 eV. The second ATI peak is of smaller amplitude and thus does not modify the results at $I_M \ll 10^{14}$ W/cm^2.

The data in Fig. 2 can be directly compared to the photoelectron energy spectrum measured by Rottke *et al.* (dashed line). We see that our theoretical peaks are slightly shifted towards the lower-energy side by less than 4% from the experimental positions. However, the disagreement is so small that it does not appear to be significant. Thus from the results of Fig. 2 we can reasonably consider that the position and the amplitude of the F peaks are in good agreement with those measured by Rottke *et al.* [18]. It seems that our computed $6F$ peak is a little higher than it should be. The theoretical widths are narrower than the experimental ones by about 20%. These results also are in reasonable agreement since the measurements are affected by the broadening due to the instrumental resolution of the analyzer.

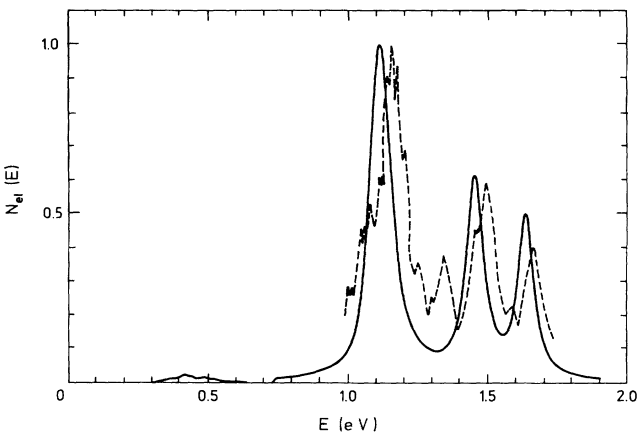

FIG. 2. Electron population $N_{el}(E)$ vs photoelectron energy E for ionization of H by 0.5-psec Gaussian pulse with peak intensity 10^{14} W/cm^2 and wavelength $\lambda=608$ nm (solid line). The first ATI peak is around 0.41 eV. The position, the normalized amplitude, and the width of the resonant structures are, respectively, 1.12 eV, 1, and 0.1 eV for the $4F$ peak; 1.46 eV, 0.6, and 0.08 eV for the $5F$ peak; 1.64 eV, 0.5, and 0.07 eV for the $6F$ peak. $N_{el}(E)$ has been normalized with respect to the number of electrons at the energy 1.12 eV (maximum of the $4F$ peak). The dashed line represents the profile of the higher-energy part of the experimental spectrum. We thank D. Feldmann for kindly providing us detailed spectra.

Furthermore the photoelectron spectrum we have computed for the resonances involving the F states is consistent with that calculated by Dörr, Potvliege, and Shakeshaft [12]. Note that the results obtained from Floquet calculations by Potvliege, Shakeshaft, and Dörr [16] are slightly shifted towards higher energies.

Another interesting aspect of the ionization process may be approached in calculating the electron rate $N_{el}(E)$ as a function of intensity I_M, for fixed pulse duration $d=0.5$ psec. In this case the laser energy varies with the peak intensity I_M. Perusal of Fig. 3 shows that the electron spectrum is significantly modified as the intensity increases. At low intensity $[I_M<I_R(t_R)]$ the resonances cannot occur and the electrons are only created around 0.41 eV, in the first ATI peak, by seven-photon-ionization process [Fig. 3(a)]. At higher intensities, the ATI peak does not move further, confirming that the shift is saturated. Although the genuine number of electrons becomes larger and larger, the relative amplitude of the ATI peak progressively decreases as the physical conditions for resonance are fulfilled. This effect can be seen in Figs. 3(b)–3(d) where the $6F$, $5F$, and $4F$ peaks successively appear as the laser intensity goes through the resonant values $I_R^{(k)}$. At intensity $I_M=5\times10^{13}$ W/cm^2, Fig. 3(d) shows that the amplitudes of the peaks increase with electron energy. This ordering of the peak amplitudes is observed although the transition matrix elements and the resonant intensities $I_R(t_R)$ of the $6F$, $5F$, and $4F$ peaks are of increasing magnitudes. In every case, the ionization probabilities verify the following relation:

$$P_I^{6F}(t_{6F})<P_I^{5F}(t_{5F})<P_I^{4F}(t_{4F})\ . \tag{3.7}$$

When the intensity I_M is slightly greater than I_R^{4F} the first electrons are created in V_{4F}, but many others have already been emitted from V_{5F} and some more electrons have been produced in V_{6F}. In spite of the relation (3.7), the electron distribution in the spectrum mainly depends on the number of atoms $V_R n_0(r,z,t)$ in each volume which themselves obey the condition

$$V_{6F}\gg V_{5F}\gg V_{4F}\ . \tag{3.8}$$

At higher intensities far from the saturation conditions, the volumes V_R expand and the constraints prescribed by the inequalities (3.8) are not so restrictive. Then the relation (3.7) between the ionization probabilities prevails. It may be remarked that the $4F$ and $5F$ peaks grow up to reach the same amplitude as that of the $6F$ peak [Fig. 3(e)]; later the $4F$ peak becomes the dominant one [Fig. 3(f)] while the $5F$ peak appears to be greater than the $6F$ peak. The comparison between Figs. 3(d) and 3(f) allows us to observe this inversion in the relative peak amplitude which comes from the evolution of the V_R volumes with intensity I_M. The behavior of the peak amplitudes we have described for the $4F$, $5F$, and $6F$ levels, also is true for higher levels of the F series. At low intensities electrons are generated inside many resonant structures of weak amplitudes which emerge in the high-energy side of the spectrum. But the increase of the laser intensity blends these first electrons to those successively created by stronger resonances. The electrons produced by these new resonances spread out in larger energy ranges and overlap the primary structures which progressively disappear in the background of the spectrum. Note that such an inversion has been observed in an ATI experiment on Xe by Agostini *et al.* [7].

Near saturation, the presence of many resonances will cause the depletion of the ground-state atoms in the V_R volume. At the smallest intensities $I_R^{(k-s)}$ on the rising edge of this pulse, the populations $\bar{n}(E_{k-s})$ will be produced to the prejudice of those $\bar{n}_e(E_k)$ created at $I_R^{(k)}$. Thus one can expect that the first hint of saturation will appear in the k-resonant peak. This effect would show itself by attenuating the relative amplitude of the resonance [17].

In most experiments the laser energy is held constant while the pulse width is adjustable within a given range. This provides the possibility of observing photoelectron spectra for different pulse durations. Thus, at fixed laser energy of 0.53 mJ, we have computed the enhanced yield profiles for several values of the pulse width. These definite conditions are sufficient to determine the peak intensity I_M of the Gaussian pulse expressed in Eq. (3.6). The shape of the spectra (Fig. 4) is very similar to that shown in Fig. 3. At 5 psec ($I_M=10^{13}$ W/cm^2), the first ATI peak is at the position 0.47 eV with a width of 0.14 eV [Fig. 4(a)]. This peak is shifted towards slightly lower energy (0.41 eV) at 2 psec ($I_M=2.5\times10^{13}$ W/cm^2) [Fig.

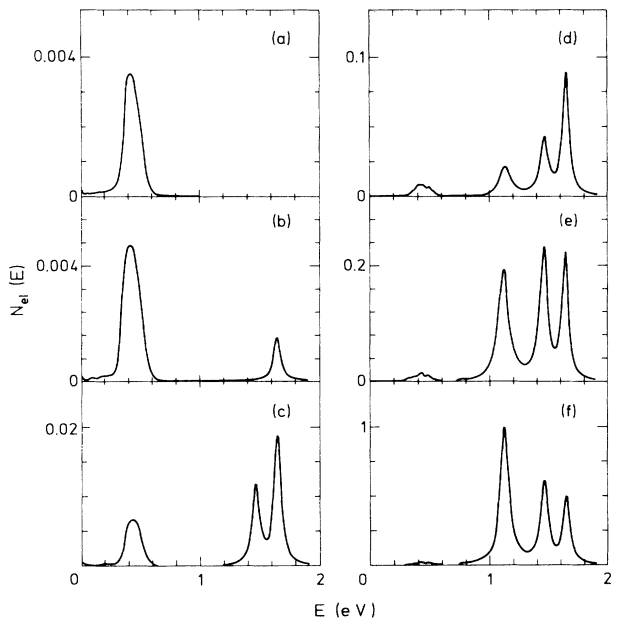

FIG. 3. Evolution of the energy spectrum of the photoelectron created by 0.5-psec Gaussian pulses with peak intensity I_M. $N_{el}(E)$ is the same as in Fig. 2. (a) $I_M=2.5\times10^{13}$ W/cm^2 is not sufficient to shift any state into resonance. The saturated first ATI peak is around 0.41 eV. (b) At $I_M=3.2\times10^{13}$ W/cm^2, the resonant $6F$ peak emerges. (c) At $I_M=4.0\times10^{13}$ W/cm^2, the $5F$ and $6F$ peaks emerge. (d) At $I_M=5.0\times10^{13}$ W/cm^2, the $4F$ peak appears. (e) At $I_M=7.0\times10^{13}$ W/cm^2 the three peaks have the same amplitude. (f) At $I_M=10^{14}$ W/cm^2, same as Fig. 2.

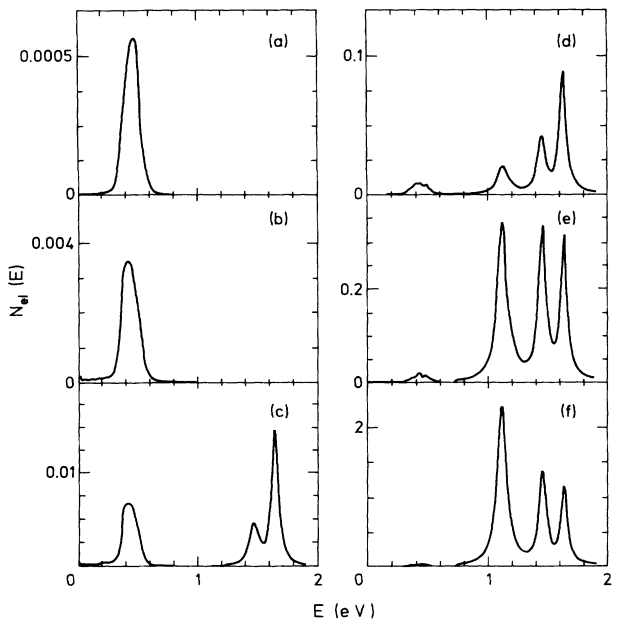

FIG. 4. Evolution of the photoelectron energy spectra produced by light pulses of constant energy (0.53 mJ), as a function of the pulse duration. (The peak intensity I_M is adjusted to get pulse of width d.) Several values of d have been selected. (a) $d=5$ psec, $I_M=10^{13}$ W/cm^2; the first ATI peak appears around 0.47 eV (width equals 0.14 eV). (b) $d=2$ psec, $I_M=2.5\times10^{13}$ W/cm^2; at the position 0.41 eV the first ATI peak is saturated (width equals 0.16 eV). (c) $d=1.3$ psec, $I_M=3.8\times10^{13}$ W/cm^2. (d) $d=1$ psec, $I_M=5\times10^{13}$ W/cm^2. (e) $d=0.6$ psec, $I_M=8.3\times10^{13}$ W/cm^2. (f) $d=0.3$ psec, $I_M=1.7\times10^{13}$ W/cm^2; one observes that the shape of the curve is very similar to that in Fig. 2.

4(b)] and the width is increased (0.16 eV). In Fig. 4(b), I_M lying inside the intensity range corresponding to the eight-photon-ionization process, the shift and the broadening of the ATI peak created by seven-photon absorption are saturated. However, the population in the peak continues to increase with the intensity I_M and consequently with the relevant interaction volume. In agreement with an experiment [2], the results in Figs. 4(a) and 4(b) show the effect of the intensity-dependent laser width on the ionization probability. To be detected, the broadening must be measured in nonsaturated ATI spectra before peak suppression. For pulse durations within the time interval (1.7 to 1 psec) the resonant structures successively appear [Figs. 4(c) and 4(d)]. The peak inversion occurs at about 0.6 psec [Fig. 4(e)] and at shorter pulse widths one gets the typical resonance features depicted in Figs. 2 and 4(f). By comparing these two last spectra one notes that the peak amplitudes do not significantly change as the pulse duration decreases from 0.5 to 0.3 psec.

IV. CONCLUSION

The aim of the paper was to present a quantitative analysis of resonances which can arise in the photoelectron energy spectrum obtained from above-threshold ionization experiments. Within the resolvent formalism, general expressions have been set up for the resonant probability density. We have demonstrated that simplified formulas, appropriate to investigate the resonant ionization of H at 608 nm, could be derived from our all-order *ab initio* theory. These analytical expressions have allowed us to discuss the role played by intensity, laser width, transition coupling, damping term, and time in the distribution of the electrons in the spectrum. To make a correct evaluation of the electron population $\bar{n}_e(E)$, it has been necessary to examine carefully, inside the interaction volume, the spatial location of the atoms which may be ionized at each intensity I_R. Then we have been led to define a set of nested effective volumes V_R which are responsible for the noticeable evolution of the resonant structures in the yield-intensity profiles (Fig. 3). We have observed an interesting behavior of the spectra which can be understood in the following way. When the first electrons are created in the $4F$ peak, the $5F$ peak is already populated and the number of electrons in the $6F$ peak is still greater than that in the $5F$ peak. As the resonant ionization probabilities $P_I(nF)$ increase when n decreases, the amplitudes of the peaks equalize for the intensity I_M around 7×10^{13} W/cm^2 and, at higher intensity, the $6F$ peak decreases more rapidly than the $5F$ peak and still much more quickly than the $4F$ peak. Then the shape of the spectrum is not appreciably modified when the intensity increases. Note that the typical spectra in Figs. 2 and 4(f) are in good agreement with those which have been measured in H. In addition, the intensity-dependent evolution of our spectra reproduces what is observed in experiment in Xe. The method we have used is also appropriate for comparing the nonresonant populations in the ATI peaks to the resonant ones located in the structures. The very large interaction volume gives rise to many nonresonant electrons which generate the background of the spectrum. These electrons contribute to the depletion of the atoms in the effective volumes V_R which lead to saturation. Since we have not taken account of the resonant structures related to the third, the fourth, etc. ATI peaks which also take part in the depletion of the ground-state atoms, we cannot estimate the distortion of the structures due to saturation and the variation of the electron yield as a function of pulse duration.

[1] P. Agostini, F. Fabre, G. Mainfray, G. Petite, and N. K. Rahman, Phys. Rev. Lett. **42**, 1127 (1979); P. Kruit, J. Kimman, and M. Van der Wiel, J. Phys. B **14**, L597 (1981); P. Agostini, M. Clément, F. Fabre, and G. Petite, *ibid.* **14**, L491 (1981); G. Petite, F. Fabre, P. Agostini, M. Crance, and M. Aymar, Phys. Rev. A **29**, 2677 (1984); Y. Gontier, M. Poirier, and M. Trahin, J. Phys. B **13**, 1381 (1980); Y. Gontier and M. Trahin, *ibid.* **13**, 4383 (1980); Z. Deng and J. H. Eberly, J. Opt. Soc. Am. B **2**, 486 (1985); G. Petite, P. Agostini, and H. G. Muller, J. Phys. B **21**,

4097 (1988); numerous references can be found in the mentioned papers.
[2] R. R. Freeman, P. H. Bucksbaum, H. Milchberg, S. Darack, D. Schumacher, and M. E. Geusic, Phys. Rev. Lett. **59**, 1092 (1987).
[3] J. Morellec, D. Normand, and G. Petite, Phys. Rev. A **14**, 300 (1976).
[4] Y. Gontier, N. K. Rahman, and M. Trahin, Phys. Rev. Lett. **34**, 779 (1975); Phys. Rev. A **37**, 4694 (1988).
[5] Z. Bialynicka-Birula and I. Bialynicki-Birula, Phys. Rev. A **14**, 1101 (1976); S. N. Dixit and P. Lambropoulos, *ibid.* **19**, 1576 (1979); M. Gavrila and J. Z. Kaminski, Phys. Rev. Lett. **52**, 613 (1984); K. C. Kulander, Phys. Rev. A **36**, 2726 (1987); J. Javanainen, J. H. Eberly, and Q. Su, *ibid.* **38**, 3430 (1988); M. Dörr, R. M. Potvliege, and R. Shakeshaft, J. Opt. Soc. Am. B **7**, 433 (1990).
[6] Y. Gontier, N. K. Rahman, and M. Trahin, Phys. Rev. A **14**, 2109 (1976).
[7] P. Agostini, A. Antonetti, P. Breger, M. Crance, A. Migus, H. G. Muller, and G. Petite, J. Phys. B **22**, 1971 (1989).
[8] H. Rottke, B. Wolff, M. Tapernon, K. H. Welge, and D. Feldmann, Z. Phys. D **15**, 133 (1990).
[9] H. Rottke, B. Wolff, M. Brickwedde, D. Feldmann, and K. H. Welge, Phys. Rev. Lett. **64**, 404 (1990).
[10] H. Rottke, B. Wolff, M. Tapernon, D. Feldmann, and K. H. Welge, in *Fundamentals of Laser Interactions II,* edited by F. Ehlotzky, Lectures in Theoretical Physics Vol. 339 (Springer-Verlag , Berlin, 1989), pp. 25–36.
[11] P. Agostini, P. Breger, A. L'Huillier, H. G. Muller, and G. Petite, Phys. Rev. Lett. **63**, 2208 (1989).
[12] M. Dörr, R. M. Potvliege, and R. Shakeshaft, Phys. Rev. A **41**, 558 (1990).
[13] Y. Gontier and M. Trahin, J. Phys. B **22**, 2531 (1989).
[14] Y. Gontier and M. Trahin, J. Opt. Soc. Am. B **7**, 463 (1990).
[15] T. J. McIlrath, R. R. Freeman, W. E. Cooke, and L. D. Van Woerkom, Phys. Rev. A **40**, 2770 (1989).
[16] R. M. Potvliege, R. Shakeshaft, and M. Dörr, in *Abstracts of the International Conference on Multiphoton Processes ICOMP V,* edited by G. Mainfray and P. Agostini (Centre d'Etudes de Saclay, Gif sur Yvette, France, 1990), p. 157.
[17] L. D. Van Woerkom, R. R. Freeman, W. E. Cooke, and T. J. McIlrath, J. Mod. Opt. **36**, 817 (1989).
[18] H. Rottke, B. Wolff, D. Feldmann, and K. H. Welge (private communication).